AGU ADVANCING EARTH AND SPACE SCIENCE

Water Resources Research

COMMENTARY
10.1029/2021WR031451

Key Points:

- Well aquifers, even with little amount of shale (~5%), might have strong anisotropy and heterogeneity and deviate from the ideal models
- The more shale content in the aquifer lithology the larger the deviation occurs
- Further call for us to avoid setting the observation aquifers onto the shale (low permeability, friability, and anisotropy) layers

Correspondence to:
L.-Y. Fu and A. Zhu,
lfu@upc.edu.cn;
aiyuzhu@cea-igp.ac.cn

Citation:
Zhang, Y., Fu, L.-Y., Zhu, A., Zhao, L., Qi, S., Huang, T., et al. (2023). Anisotropy and heterogeneity induced by shale in aquifer lithology—Influence of aquifer shale on the leaky model with tidal response analysis. *Water Resources Research*, *59*, e2021WR031451. https://doi.org/10.1029/2021WR031451

Received 21 OCT 2021
Accepted 26 JAN 2023

Author Contributions:
Data curation: Yuchuan Ma, Wang Zhang
Formal analysis: Shengwen Qi
Investigation: Yuchuan Ma
Methodology: Aiyu Zhu, Lianfeng Zhao
Software: Aiyu Zhu, Lianfeng Zhao
Writing – review & editing: Aiyu Zhu, Shengwen Qi, Tianming Huang

Anisotropy and Heterogeneity Induced by Shale in Aquifer lithology—Influence of Aquifer Shale on the Leaky Model With Tidal Response Analysis

Yan Zhang[1,2,3], Li-Yun Fu[4,5], Aiyu Zhu[6], Lianfeng Zhao[2,7], Shengwen Qi[1,2,8], Tianming Huang[1,2,8], Yuchuan Ma[9], and Wang Zhang[2,7,10]

[1]Key Laboratory of Shale Gas and Geoengineering, Institute of Geology and Geophysics, Chinese Academy of Sciences, Beijing, China, [2]Innovation Academy for Earth Science, Chinese Academy of Sciences, Beijing, China, [3]Department of Earth and Planetary Science, University of California, Berkeley, CA, USA, [4]Shandong Provincial Key Laboratory of Deep Oil and Gas, China University of Petroleum (East China), Qingdao, China, [5]School of Geosciences, China University of Petroleum (East China), Qingdao, China, [6]Institute of Geophysics, China Earthquake Administration, Beijing, China, [7]Key Laboratory of Earth and Planetary Physics, Institute of Geology and Geophysics, Chinese Academy of Sciences, Beijing, China, [8]University of Chinese Academy of Sciences, Beijing, China, [9]China Earthquake Networks Center, Beijing, China, [10]State Key Laboratory of Lithospheric Evolution, Institute of Geology and Geophysics, Chinese Academy of Sciences, Beijing, China

Abstract Tidal and barometric water-level responses in wells have been widely used to calculate the hydraulic properties of aquifer systems. The effect of anisotropy induced by shale content on such responses has not received significant attention. In this study, we examine how the presence of shale (anisotropy, extremely low porosity/permeability; approximately 10^{-4} to 10^{-3} mD), which occurs as interlayers in aquifers, affects the tidal responses of the leaky model. Our findings show that the number of wells with shale in the screened section of the study aquifer is limited. Here, we focus on the study of the limited number of wells in the North China Platform to ensure a similar geological background for each well. Calculations indicate that wells, even with a small amount of shale (≥~5%) in the observation aquifer, may exhibit strong anisotropy and heterogeneity, deviating from the theoretical analytical solutions obtained using isotropic and homogeneous assumption models. Generally, the higher the shale content in aquifer lithology, the greater the phase shifts deviated. Thus, theoretical ideal models with isotropic and homogeneous assumptions may only obtain a rough estimation for wells with shale in aquifer lithology, suggesting that we avoid setting observation aquifers onto shale layers.

Plain Language Summary As special lithology, shale is fragile, compact, and anisotropic, and because of its extremely low porosity/permeability (10^{-4} to 10^{-3} mD), it will also induce the heterogeneity of the whole layer containing both shale and other lithology rocks. Therefore, aquifers containing shale might exhibit unique characteristics. However, there is mostly no previous research on this topic in the hydro-geophysics region, perhaps because the number of wells with shale in aquifer lithology is very limited.

1. Introduction

Hydro-mechanical processes have dominating control on permeability evolution (Anyim & Gan, 2020; Cai et al., 2017). Water-level responses to barometric pressure and tidal strain are used to calculate vertical permeability and judge the confinement extent of aquifers (e.g., Rojstaczer, 1988; Wang et al., 2018; Q. Y. Yang et al., 2021; H. Zhang, Shi, et al., 2019; Y. Zhang, Wang, et al., 2019). The leaky model of tidal response (Wang et al., 2018) has been tested by groundwater wells in the North China Platform, for the first time, with both the M2 and O1 tidal waves and without any pre-set parameters. Most of those wells are semi-confined, even with a deep aquifer, and covered with thick mudstone/shale (Y. Zhang et al., 2021). The barometric response (of water level) model (Rojstaczer, 1988) has also been widely used to calculate horizontal and vertical hydraulic parameters (e.g., Hussein et al., 2013; H. Zhang, Shi, et al., 2019), but several parameters always need to be pre-set, such as the storage coefficient of aquifers and aquitards, making the model not completely independent, even if the pre-set parameters may not have obvious impacts. Although both models are widely used, the effect of lithology on such responses has not attracted much attention, especially for the shale (low porosity-low permeability, fragility, and anisotropy) layers in aquifers. Wang and Manga (2021) compared the analytical solution of both the tidal

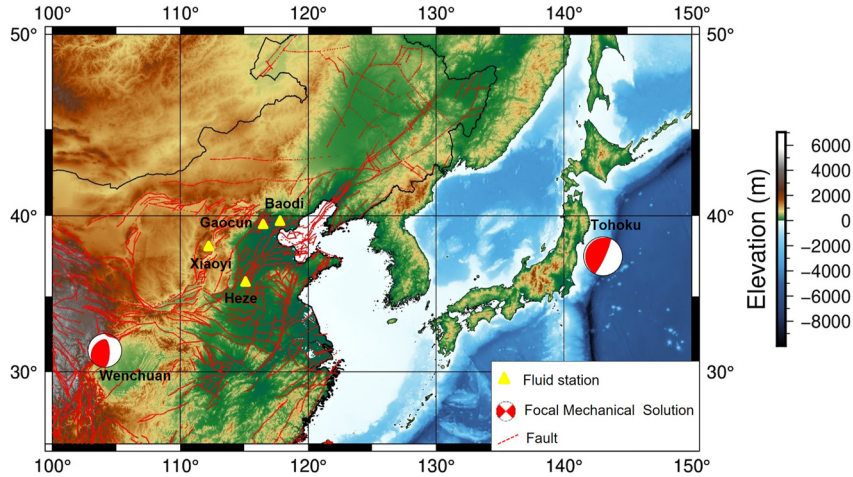

Figure 1. Locations of the study groundwater wells (GC, BD, XY, and HZ) on the North China Platform, the epicenters of the 2008 M_w 7.9 Wenchuan earthquake and the 2011 M_w 9.1 Tohoku earthquake (from Global CMT). The "beach balls" show the focal mechanism for earthquakes. The red lines indicate the surface faults (Deng et al., 2004); the yellow triangles indicate the fluid stations.

response leaky model of Wang et al. (2018) and the barometric response model of Rojstaczer (1988) and found that they are the same; therefore, their results should be approximately similar (Y. Zhang et al., 2022).

In this study, we examine how the presence of shale, which occurs as interlayers in aquifers, affects the tidal response leaky model of Wang et al. (2018). Calculations and comparisons indicate that wells even with a small amount of shale (>∼5%) in the screened section of an aquifer may exhibit strong anisotropy/heterogeneity and will deviate from the ideal analytical solution of the tidal response leaky model. Hence, the leaky model may only perform rough estimations. Therefore, observation aquifers should not be set onto lithologies that contain shales.

According to Wang et al. (2018), for the tidal response leaky model, phase shifts are significantly more sensitive to permeability variations than amplitude ratios; thus, we focused on the analysis of phase shifts in this paper. Similarly, the study by Y. Zhang et al. (2021) also focused on the calculation of phase shifts.

2. Selection Principles and Observations

Water-level responses are used to estimate hydraulic properties (S, T, and K') (Appendix A) based on the tidal responses of water level using the leaky model of Wang et al. (2018), which assumes an aquifer is isotropic and overlain by a leaky confining layer. Re-substituting the obtained S, T, and K' into the analytical solution of the leaky model (eq. A8 of Appendix A), we could obtain the deduced phase shifts (see Figure 5). As a pretest, we found that the difference between the deduced phase shifts obtained using the model and the on-site phase shifts was low for data from a well penetrating a relatively homogeneous aquifer of sandstone. However, the difference between the deduced and on-site phase shifts increases with an increase in shale content in the aquifer section. This leads us to infer that the deviation of the phase shift is due to the anisotropy caused by shale in the aquifer. Hence, in this paper, we intend to testify this issue.

Statistics show that the number of wells with shale in the screened section of the aquifer is limited (Seismic Monitoring Records of China, 2002–2007). This is probably due to the low permeability/porosity (Zhao et al., 2018), friability, and anisotropy, and observation aquifers of groundwater wells are always avoided to set onto shale/mudstone layers. Here, we focus on the study of wells in the North China Platform to ensure a similar geological background for each well.

Data from the four wells (Figure 1) with shale in the aquifer lithologies, along with relatively continuous water-level data, were collected from 2008 to 2011 so that the data can include responses to the 2008 Wenchuan and 2011 Tohoku huge earthquakes (Figure 2). The four selected wells are more than 100 km away from the ocean, so oceanic tides, which have an impact tens of kilometers away from the coast, are avoided (Beaumont & Berger, 1975).

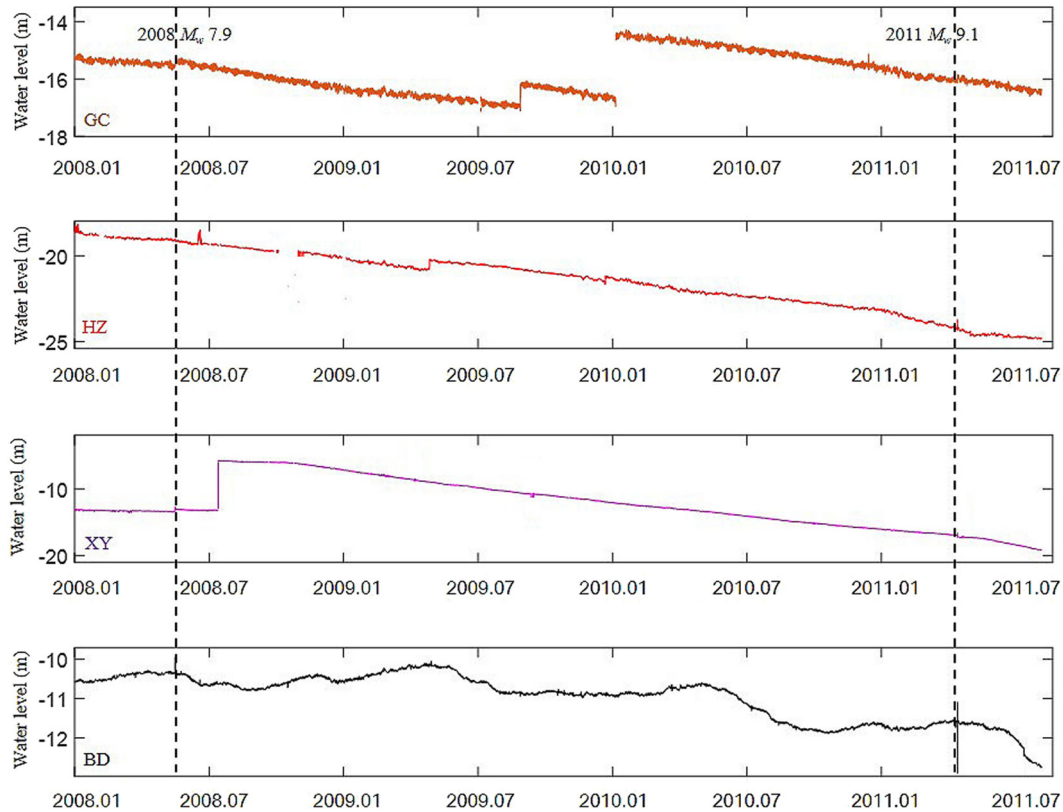

Figure 2. Original water level of wells GC, HZ, XY, and BD from January 1, 2008, to June 30, 2011. The gaps indicate invalid original data records. The vertical dashed lines represent the start time of the 2008 Wenchuan and the 2011 Tohoku huge earthquakes, which had no obvious influence on the water level (as indicated by Y. Zhang et al. (2021), all those wells are leaked). These four wells are non-artesian; thus, the *y*-coordinate axis indicates the distance from the water-level surface to the ground.

The Mapseis software (Lu et al., 2002) is used to calculate the theoretical tidal strain, which has been satisfactorily compared against a widely used software package Baytap-G (see Supplement-S2 of Y. Zhang et al. (2021)). The water level was observed using an LN-3A digital water-level instrument with observational accuracy of ≤0.2% F.S., a sampling rate of 1 sample/min, and a resolution ratio of 1 mm. Basic information about these wells is shown in Table 1.

Table 1
Basic Information of the Four Wells

Station	Major aquifer lithology	Well diameter/mm	Well depth/m	Length of aquifer/m	Length of aquitard/m	Epicentral distance/km		Geological structure
						Wenchuan	Tohoku	
Gaocun	Limestone	240	3,402.81	717.30	2,685.50	1,478.00	1,894.02	Northern part of Jizhong cavity
Heze	Limestone, dolostone, and shale	216	2,001.00	862.00	1,138.00	500.48	819.77	Luxi'nan plain, east side of the Liaokao fault
Xiaoyi	Sandstone and muddy shale	150	502.93	102.93	400.00	1,062.08	3,258.51	Jiaocheng fault
Baodi	Limestone, dolostone, and shale	350	427.17	217.00	105.00	1,469.55	1,745.84	Intersection of Yanshan mountain alluvial plain and Jizhong hollow

Table 2
Volume Ratio of Shale in the Observation Aquifer

Station	Thick of shale layer/m (average)	Thick of shale layer/m (maximum)	Thick of shale layer/m (minimum)	Aquifer thickness/m	Volume ratio of shale (average)	Volume ratio of shale (maximum)	Volume ratio of shale (minimum)	Error of volume ratio of shale
Gaocun	**0**	0	0	717.30	**0**	0	0	/
Heze	**60.14**	70.16	50.12	862.00	**6.98%**	8.14%	5.81%	1.16%
Xiaoyi	**23.80**	26.22	21.38	102.00	**23.33%**	25.70%	20.96%	2.37%
Baodi	**87.00**	121.57	52.43	217.00	**40.09%**	56.02%	24.16%	15.93%

3. Lithological Logs of Study Wells

For well Gaocun, shale is absent in the aquifer lithology (Y. Zhang et al., 2021), and thus, the shale content of the aquifer for this well is 0%. Conversely, the shale content of well Heze is 6.90%, well Xiaoyi 23.33%, and well Baodi 40.09% (see Section 3.1; Table 2). The lithological logs of the study wells are shown in Figure 3, as recorded in the Seismic Monitoring Records of China (2002–2007). Red lines and numbers show the study aquifer and the depth of the screened section (Figure 3).

3.1. Calculation Rules of Shale Content

1. For well Heze, the screened section is 1,138–2,000 m, and the measured shale in layers ranges from 1,929.84 to 1,949.88–2,000 m (Figure 3); thus, the volume ratio of shale is approximately (2,000−1,949.88)/(2,000−1,138) = 5.81% to (2,000−1,929.84)/(2,000−1,138) = 8.14% of the screened section; the average volume ratio of shale is (5.81%+8.14%)/2 = 6.98%, with a small error of ±1.16% (Table 2);
2. For well Xiaoyi, the shale layer (405.13–438.05 m; 468.94–484.35 m; 489.16–502.93 m) is composed of two substances in the screened section (400–502.93 m) (Figure 3). Thus, we assume that the volume ratio of each substance is ½ in the shale layer. Meanwhile, there is muddy shale in layers between 405.13–438.05 m and 468.94–484.35 m. For muddy and sandy shale, we assume shale accounts for 60%–80%, and the other 40%–20% is quartz sandstone (C. L. Hu et al., 2014). After calculation, the average thickness of shale is 1/2 × (438.0

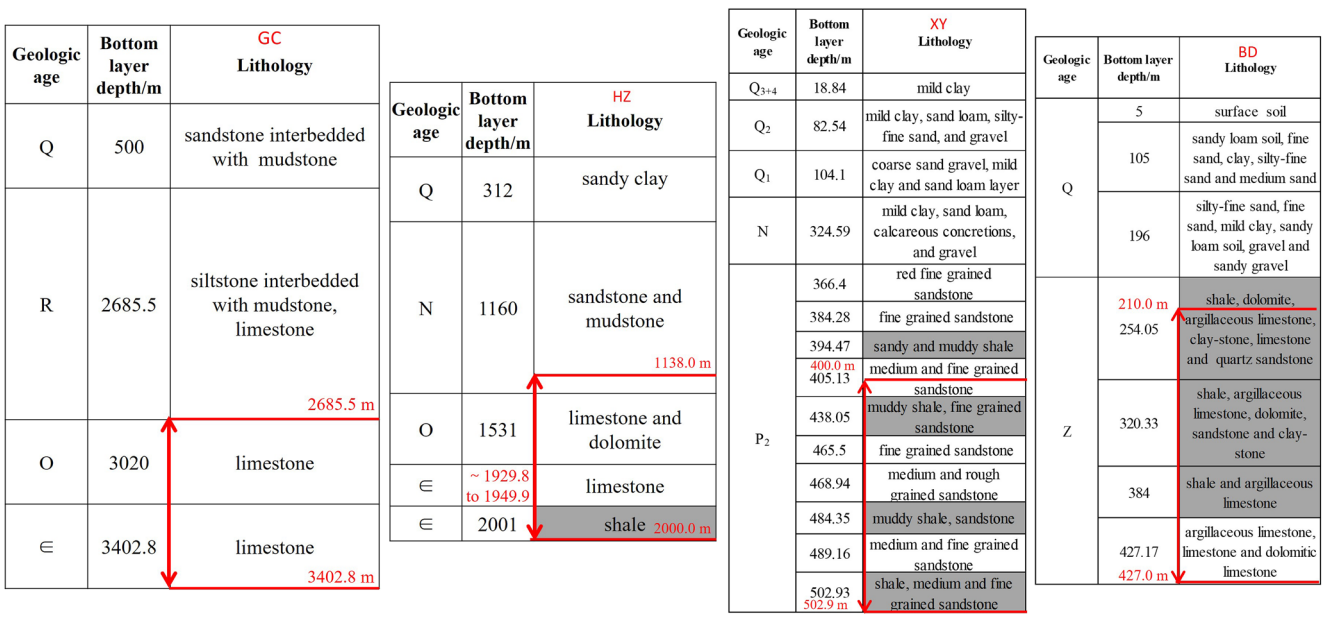

Figure 3. Well logs showing the details of rock types in the study wells. The red lines and numbers indicate the depth of the study aquifers. The dark color indicates the shale layer. To calculate the shale content in the aquifer, the description of the aquifer lithology is thoroughly detailed (Seismic Monitoring Records of China, 2002–2007).

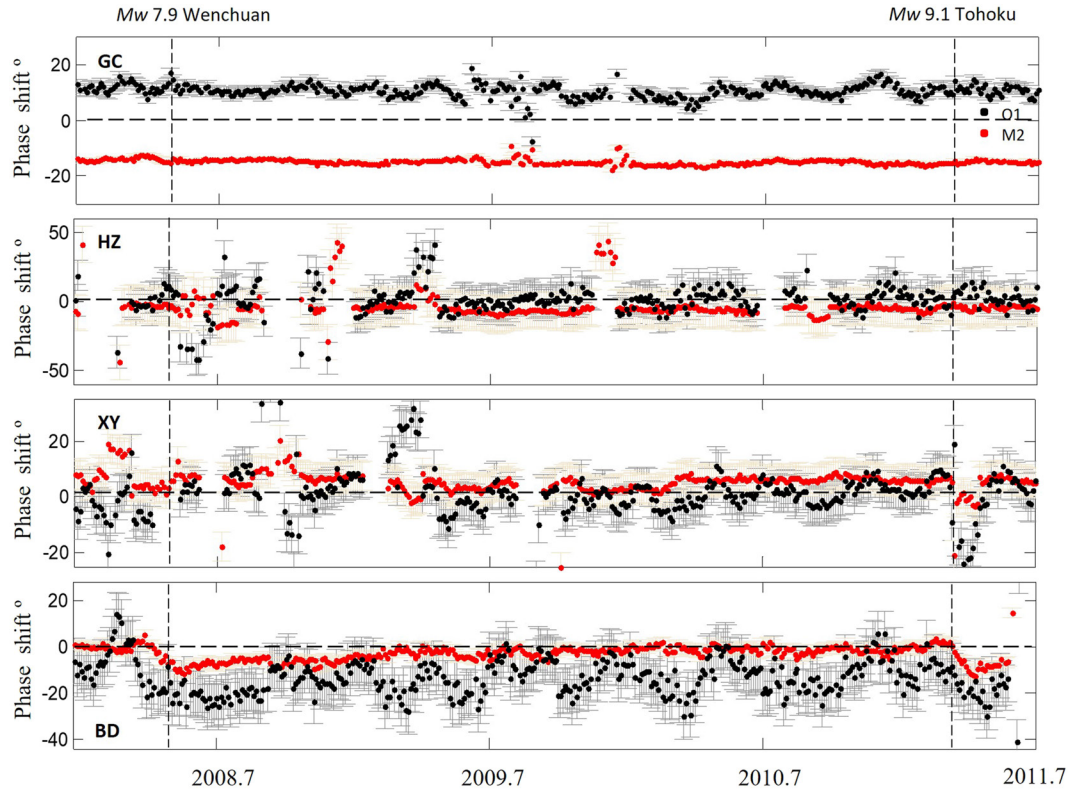

Figure 4. Phase shift to the M_2 and O_1 tides for the four study wells from 2008 to 2011. The vertical lines indicate the occurrence time of the 2008 Wenchuan and the 2011 Tohoku huge earthquakes. (Modified from Y. Zhang et al. (2021)).

5–405.13) × (0.6 + 0.8)/2 + 1/2× (484.35–468.94) × (0.6 + 0.8)/2 + 1/2 × (502.93–489.16) = 23.80 m; thus, the volume ratio of shale is 23.8/(502.93–400) = 23.33%, with an error of 2.37% (Table 2);

3. For well Baodi, the screened section is 210–427 m (Figure 3), and different shale layers contain different types and numbers of substances. There are six substances in the shale layer 210–254.05 m, and because shale comes as the first substance, the volume ratio of shale is assumed to be between 1/6 and 5/6 in this layer; the volume ratio of shale is assumed to be between 1/5 and 4/5 in the layer 254.05–320.33 m, in which there are five substances. It is assumed that shale accounts for ½ in layer 320.33–384 m, in which there are only two substances. After calculation, the average thickness of shale is (1/6 + 5/6)/2 × (254.0 5–210) + (1/5 + 4/5)/2 × ((320.33–254.05) + 1/2 × ((384–320.33) = 87.00 m, and the volume ratio of shale is 87.00/(427−210) = 40.09% with an error of ±15.93% (Table 2).

4. Tidal Response Analysis

4.1. Tidal Response of Water Level

Mapsis (Lu et al., 2002) software is used, as in previous studies, to analyze the water-level response to earth tides. As described by Y. Zhang et al. (2021), a moving time window of 30 days and a running step of 3 days were also used. The M_2 and O_1 tidal components are used because of their relatively small barometric effects and large amplitudes (e.g., Barbour et al., 2019; Hsieh et al., 1987). Meanwhile, without the resonances incurred by the thermal effect or the free core nutation, the M_2 phase is more accurate than the O_1 phase (Doan et al., 2006).

As shown in Figure 4, in the GC well (aquifer shale content 0%), the phase shifts of O_1 are positive (˜ 15°) and those of M_2 are negative (˜ −15°), with all phase shifts of O_1 larger than those of M_2; in wells HZ (aquifer shale content 6.98%) and XY (aquifer shale content 23.33%), most of the phase shifts are approximately 0, and phase shifts of O_1 are larger than those of M_2 for well HZ for most dots, whereas the opposite is true for well XY. In well BD (aquifer shale content 40.09%), the phase shift is nearly 0 to the M_2 tide and nearly −20° to the O_1 tide; thus, most of the phase shifts of O_1 are smaller than those of M2.

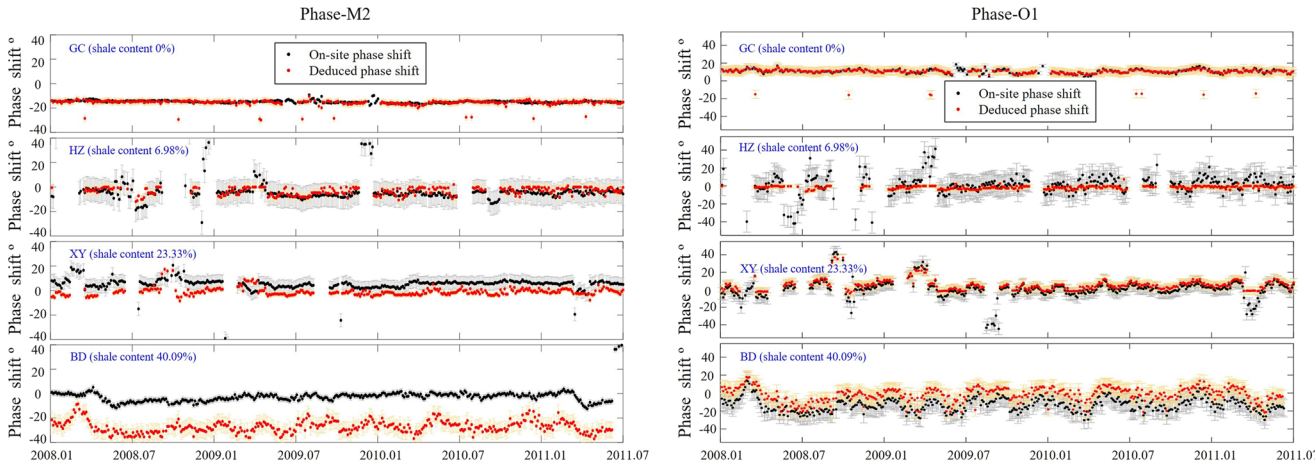

Figure 5. Comparison between the phase shifts obtained from the on-site observed water level (black dots) (the same as Figure 4) and those deduced from the analytical solution of the tidal response leaky model with the obtained parameters (S, T, and K') (red dots) for the O_1 and M_2 tides for each well. (Because of the simplification of the tidal response leaky model, there are neglected kick points in the inversed parameters of S, T, and K' (Y. Zhang et al., 2021), and thus, there are also neglected kick points in the deduced phase shifts (red dots).).

4.2. Deviation From the Tidal Response Leaky Model

The tidal response leaky model (Wang et al., 2018) (Appendix A) was used to simulate a system of an aquifer and aquitard (two-layer model), with each aquifer and aquitard layer assumed to be isotropic and homogeneous. This model has three independent parameters: the transmissivity T and storage coefficient S of the aquifer, and vertical hydraulic conductivity K' of the aquitard. The phase shifts of the M_2 and O_1 tidal responses of water level and the amplitude ratio of M_2 wave to O_1 wave were used as the three inputs. In short, three inputs were used to obtain these three parameters (S, T, and K') (Appendix A). Finally, the best solution for each well was found using least squares optimal fitting and nonlinear, least squares inversion code (Fsolve, https://www.mathworks.com/help/optim/ug/fsolve.html) (Y. Zhang et al., 2021). Although, this model is called the tidal response leaky model, it also could be applied to wells with no leakage, which is in accordance with $K' = 0$ (Wang et al., 2018), and which is identical to the classical solution for a perfectly confined aquifer of Hsieh et al. (1987). Published parameters for rocks of the same lithology as the aquifers and aquitards (Figure 3) are used as the initial values in the inversion, thereby constraining the inversion (Y. Zhang et al., 2021). As calculated by Y. Zhang et al. (2021), the study wells in the North China Platform leaked with a value of K', except well HZ, which leaked with an extremely small value of $K' \sim 10^{-10}$ (m/s) (none leakage, values of 10^{-10} (m/s) were assigned when K' approached 0 in the least squares inversion because K' could be in the denominator in the software), and could be perceived as confined wells (H. F. Yang et al., 2021) (Appendix A). Inverted results of T and K' for each well have been compared with the laboratory measurements and the barometric efficiencies and verified to be reasonable (Y. Zhang et al., 2021). Perhaps, the specific storages (S_s) are not significant, so the laboratory measurements are lacking, and only 1 order of magnitude could be obtained for one specific lithology (Wang, 2000), making it difficult to justify.

Furthermore, substituting the inverted S, T, and K' into the analytical solution equations (Equations A6, A7, and A9—Appendix A), the phase shifts to the O_1 and M_2 tides are deduced using the ideal leaky model (red dots in Figure 5). To identify the mismatches between the tidal response leaky model of Wang et al. (2018) and the on-site situation of each well, we compared the phase shifts deduced using the tidal response ideal leaky model and the phase shifts in the original observation data (Figure 5).

4.2.1. Deviation for the M_2 Tide

For the M_2 tide, the phase shifts deduced using the tidal response leaky model (red dots) and the original phase shifts (black dots) calculated from the water-level on-site observations for well GC are similar across the entire data set, and the phase shifts are essentially constant (Figure 5, above). For well HZ, there are brief, large fluctuations in the on-site phase shifts, but these variations are not explained by the ideal leaky model (Figure 5, above). For well XY, the ideal leaky model predicts phase shifts systematically more negative by approximately

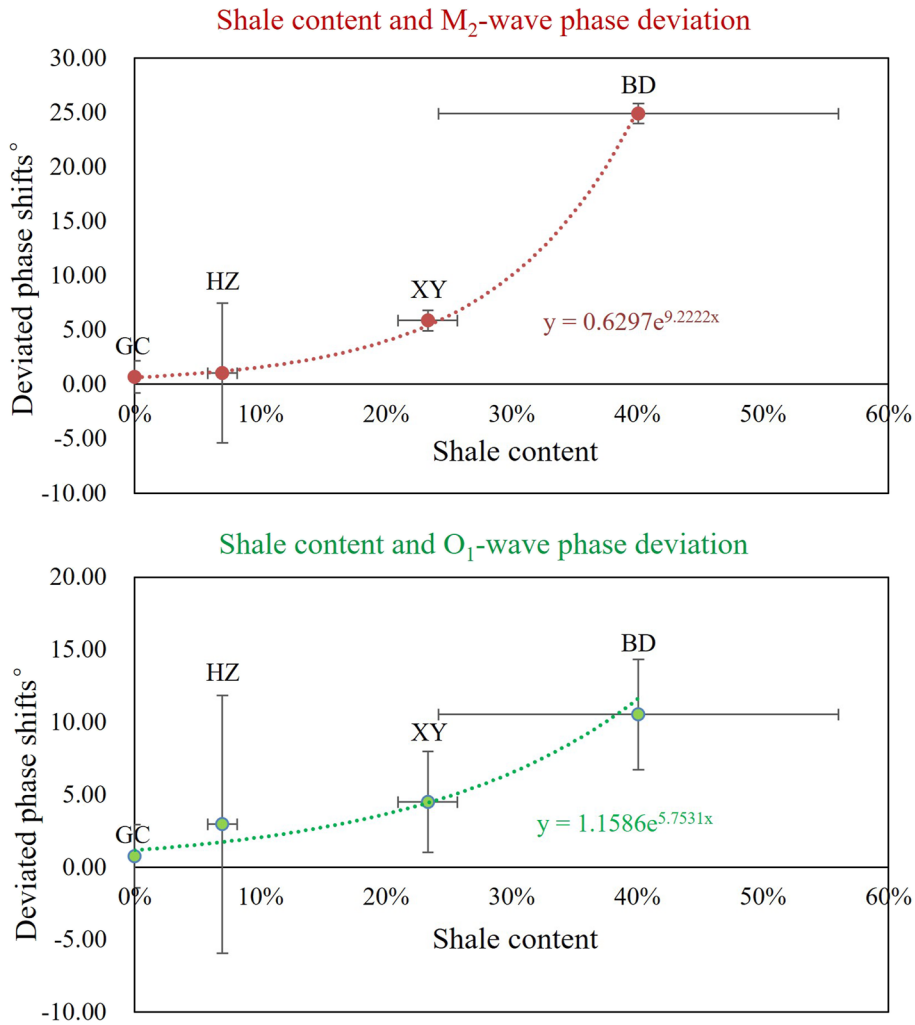

Figure 6. Relation between shale content and the deviation of phase shifts of the M_2 and O_1 waves. Generally, the higher the shale content in the aquifer, the greater the inversed phase shifts deviated. Here, we only calculated the absolute value of the deviation of phase shifts and not care about the positive or negative deviation, which could be very complex and break the obvious rule.

10° than the on-site observation phase shifts (Figure 5, above). For well BD, the predicted phase shifts are also consistently behind the observed phase shifts, but the difference is greater than that for well XY (Figure 5, above). Generally, the higher the shale content, the larger the deviation of the phase shifts (Figure 6, above) for the M_2 tide.

4.2.2. Deviation for the O_1 Tide

The results for the O_1 tide at well GC are similar to those for the M_2 tide but are different at the other wells (Figure 5, below). For example, for well HZ, the on-site phase shifts from the observation data for the O_1 tide are highly variable and erratic, whereas the deduced phase shifts obtained using the tidal response leaky model are fairly uniform (Figure 5, below) (mechanism and explanations, see Section 5 portion). For well XY, both the deduced and on-site phase shifts are erratic, but they are similar to each other (Figure 5, below). This differs from the M_2 data, where there is a systematic difference between the phase shifts deduced from the ideal leaky model and on-site observation data (Figure 5, above). The on-site phase shifts for the O_1 tide at well BD are systematically offset from those deduced from the ideal leaky model (Figure 5, below), as they are for the M_2 tide (Figure 5, above). However, the sign of the offset for the O_1 tide is opposite to that for the M_2 tide (Figure 5, above).

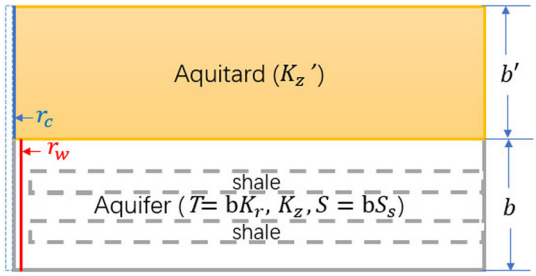

Figure 7. Schematic drawing of a multi-layer groundwater system used in the present simulation (according to the logging of well Xiaoyi). $r_c = 4.5$ cm is the case radius, and $r_w = 7.5$ cm is the well radius. The thicknesses of the aquifer and aquitard are $b = 102.95$ m and $b' = 400$ m, respectively. The transmissivity and storativity of the aquifer are denoted by T and S, respectively, where $T = b\,K_r$ and $S = b\,S_s$. K_z and K_z' are the respective vertical hydraulic conductivity of the aquifer and aquitard, which are with the same value during the numerical simulation (except for the K_z value of the shale layer; Table 3).* K_z' in this figure represents the K' in Figure A1 (Appendix A).

4.2.3. Relation Between Shale Content and the Deviation of Phase Shifts

We calculated the deviated phase shifts (in Figure 6) based on the difference in the median value of the on-site (black dots) and deduced (red dots) phase shifts in Figure 5. Generally, the higher the shale content, the greater the phase shifts deviated (Figure 6).

For the O_1 tide, the phase shifts for well HZ appear to deviate more than those for well XY (Figure 5, below), but some of the on-site phase shifts (black dots) are smaller and larger than the deduced phase shifts (red dots) for well HZ, whereas most of the on-site phase shifts (black dots) are smaller than the deduced phase shifts (red dots) for well XY (Figure 5, below), so the final average deviation of phase shifts for well XY is slightly greater than that for well HZ (Figure 6, below).

Some of the abrupt kick black dots for the on-site phase shifts for wells HZ, XY, and BD could not be explained by the ideal leaky model (red dots in Figure 5), introducing uncertainties and errors in the phase-shift deviation calculations.

4.2.4. Numerical Simulation Testing the Relation Between Shale Content and the Deviation of Phase Shifts

Based on Darcy's equation, Hantush and Jacob (1955) and Hantush (1960, 1967) derived the leaky model with a source term "-K′/b′ h" by which represents the leakage in the aquitard, this model has some simplifications, for example, the aquitard is incompressible with negligible storage and the flow across it is vertical, and so on (Wang et al., 2018). Therefore, Zhu and Wang (2020) used a multi-layered numerical model to explore the limitations of the analytical solution of the leaky aquifer model, meanwhile they used the leaky analytical solution to verify the numerical model and indicate that the numerical model can be totally reduced to the analytical solution. The numerical simulation could be precisely applied to wells with relatively thin aquifers and relatively small vertical leakage. Here, we use well Xiaoyi as an example to perform the numerical simulation and to check about the relation between shale content and the deviation of phase shifts.

As described by Zhu and Wang (2020), we use an axially symmetrical, multi-layer finite element model (Figure 7) of a groundwater system consisting of an aquifer confined above by a semi-confining aquitard, which is the same as the leaky model of Wang et al. (2018) (Appendix A Figure A1). A vertical well centered along its axis completely penetrates the aquitard and is open to the aquifer. Groundwater in the aquifer is allowed to flow in both the horizontal and vertical directions. The semi-confining aquitard is assumed to have finite transmissivity ($T' = 0$) and storativity ($S' = 0$). Groundwater flow in such a system driven by Earth tides could be evaluated by solving the differential Equation 1 (Zhu & Wang, 2020).

$$K_{ri}\left[\frac{\partial^2 h_i}{\partial r^2}+\frac{1}{r}\frac{\partial h_i}{\partial r}\right]+K_{zi}\frac{\partial^2 h_i}{\partial z^2}=S_{si}\left(\frac{\partial h_i}{\partial t}-\frac{B_i K_{ui}}{\rho g}\frac{\partial \epsilon}{\partial t}\right), \tag{1}$$

where h_i[m] is the hydraulic head in the ith layer, i increases from low (the basement) to high (the ground surface), r[m] the radial distance from the axis of the well, K_{ri}[m/s] and K_{zi}[m/s], respectively, the hydraulic conductivities in the radial and vertical directions of the ith layer, S_{si} [m^{-1}] the specific storage of the ith layer, ϵ the tidal volumetric strain, Bi and K_{ui}[Pa], respectively, the Skempton's coefficient and the undrained bulk modulus of the ith layer, [We set BKu = 10 GPa for the common aquifer layer, and BKu = 35 GPa for the shale layer (Detournay & Cheng, 1993); Since little paper records the BKu value of shale we used that of granite instead] and $\rho = 10^3$ kg/m^3 and $g = 9.8$ m/s^2, respectively, the density of water and the gravitational acceleration. K_{ri} and K_{zi}, respectively, are related to the horizontal and vertical permeabilities k_{ri} and k_{zi} of the ith layer by $K_{ri} = k_{ri}\rho g/\mu$ and $K_{zi} = k_{zi}\rho g/\mu$, respectively, $\mu = 10^{-3}$ Pa s the viscosity of water, and b_i the thickness of the ith layer.

COMSOL, a commercially available finite element software package, is also used to do the numerical simulation. We assume a boundary condition with the pore pressure $p_0 = 0$ (1 atm) on the ground surface ($z = 0$), where

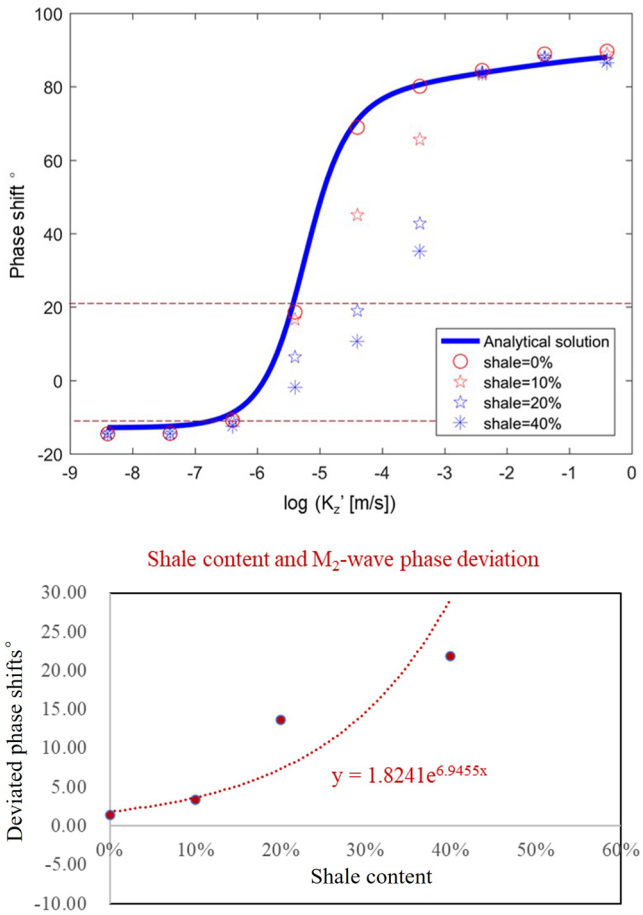

Figure 8. (a) Comparison between the numerically simulated water-level response to the M_2 tide at different shale content (0%; 10%; 20%; 40%) in the aquifer and the analytical solution (curve; Wang et al., 2018). Phase shift plotted against aquitard leakage factor K_Z' (* K_z' in this figure represents the K' in Figure A1 (Appendix A).). The more shale content, the larger the phase shifts deviated during the range of phase shifts (approximately: −10° to 20°) of the M_2 wave of well Xiaoyi (Figure 4). (b) Relation between shale content (0%; 10%; 20%; 40%) and the deviation of phase shifts of the M_2 waves in well Xiaoyi, according to dots between the dashed lines in panel a. Generally, the higher the shale content in the aquifer, the greater the inversed phase shifts deviated during the range of phase shifts (approximately: −10° to 20°) of the M_2 wave of well Xiaoyi (Figure 4). Here, we also calculated the absolute value of the deviation of phase shifts as the same as in Figure 6.

ignore the hydrostatic pressure, and assign a mixed boundary condition at the left open section of the borehole (Figure 7), which is dependent on the solution:

$$2\pi r_w T_1 \frac{\partial h_1(r,t)}{\partial r} - \pi {r_c}^2 \frac{\partial h_1(r,t)}{\partial t} = 0 \quad (2)$$

where r_w is the well radius and r_c is the case radius. Finally, we assign no-flow conditions on the left case section of the well, on the right boundary ($r \to \infty$) of the model, and at the base ($z = b + b'$) of the model. Therefore, finally, we have four boundary conditions around the four sides.

The numerical model in this paper can also be reduced to the analytical solution when the aquifer has no shale (shown in Figure 8a, shale = 0%), which proved that the numerical solution is right and the different phase shift is due to the thickness of the shale in the aquifer.

Specifically, some shale layers are distributed in the aquifer uniformly (Figure 7), the thickness of the layered shale could be regulated so that the shale content can be regulated according to our requirements (0%–10%–20%–40% in Figure 8). To indicate shale layers, properties in horizontal and vertical directions could be set according to shale properties. Material properties are prescribed in Table 3. A small element size (0.5 m) and time steps (500 s) are used to ensure accuracy and numerical stability (otherwise, the program will skip and stop). Finally, we focus on the response to the M_2 tide, which is the most widely used response because of its relatively large signal-to-noise ratio and that it is minimally affected by the changes in the barometric pressure.

Figure 8a is intended to verify the numerical model by comparing it to the analytical solution. As we can see, when the shale content is 0%, those dots are very adjacent to the analytical solution. As shown in Figure 8a, during the general range of phase shifts (approximately: −10° to 20°) of the M_2 wave of well Xiaoyi (Figure 4), with an increase in shale content in the aquifer, the deviation of phase shifts increases. To do comparison with Figure 6, we also plotted the similar Figure 8b (during the general range of phase shifts of approximately: −10° to 20°), which also indicating that the more shale content, the larger the deviation occurs in well Xiaoyi.

In this paper, since the positive or negative of phase shifts could bring complex and break the obvious rules in Figure 6, we only care about the deviation extent of the phase shifts (the absolute value of phase shifts) rather than the sign of the deviation.

Last but not least, for the tidal response leaky aquifer analytical model, it could be seemed as the 1D model, since the aquifer flow are mainly in the

Table 3
Parameters for the Numerical Simulation

Parameter	Parameter	Aquifer		Aquitard
		Shale layer	Common aquifer	
Horizontal hydraulic conductivity	K_r (m/s)	1×10^{-7}	1×10^{-7}	0
Vertical hydraulic conductivity	K_Z (m/s) for aquifer K_Z' (m/s) for aquitard	4×10^{-9}	4×10^{-9} to 4×10^{-1}	
Specific storage	Ss (1/m)	1×10^{-6}	1×10^{-6}	0
Porosity	n	0.30	0.45	0.30

Note. The vertical hydraulic conductivity of the common aquifer and aquitard is K_Z and K_Z', which varied between 4×10^{-9} and 4×10^{-1} (m/s) (Figure 8a) and $K_Z = K_Z'$ during the numerical simulation, and thus in Figure 8a, we are giving results for a wide range of K' (4×10^{-9} to 4×10^{-1} (m/s)). Shale means the shale layer in the aquifer. K_Z' in this table represents the K' in Figure A1 (Appendix A).

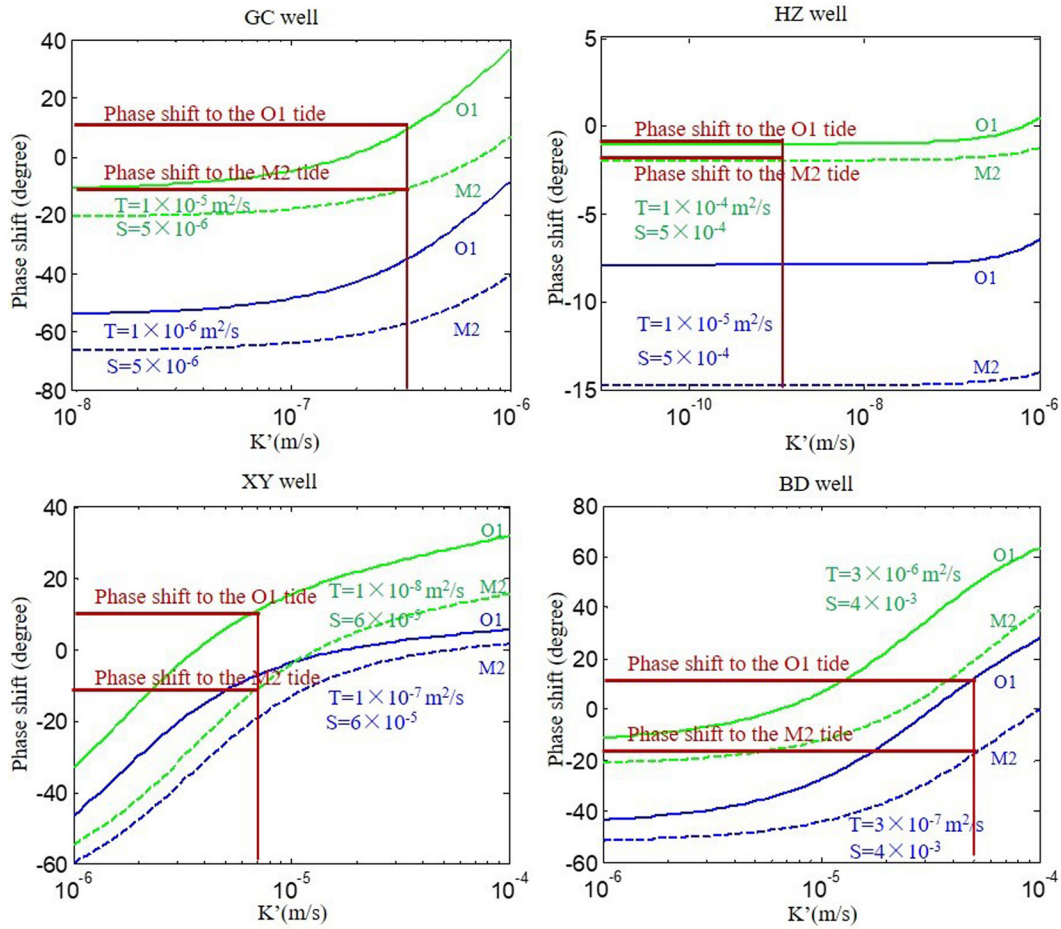

Figure 9. Theoretical prediction (curves) of the phase shift to the O_1 and M_2 tides (horizontal lines) with average inverted values of T and S in the four wells, plotted against K'. Vertical line: the average vertical hydraulic conductivity K' of each well (modified from Zhang et al. (2021)).

horizontal direction and only with the vertical leakance term; While, for the shale layer embedded leaky aquifer numerical model, it is a 2D model, and the fluid flow is set both in the horizontal direction and in the vertical direction (Table 3) in each layer in the aquifer. Meanwhile, different layers are with continuity conditions in the aquifer.

5. Discussion

5.1. Explanations for Deduced Phase Shifts Based on Analytical Solution of the Leaky Model

Based on the tidal response leaky model (Wang et al., 2018), the theoretical predictions of phase shift against K' with the inverted T and S are plotted in Figure 9 (modified from Y. Zhang et al. (2021)) according to the analytical solution.

5.1.1. Case of Well XY and BD

As shown in Figure 9, for the analytical solution of the ideal leaky model, the phase shifts of the O_1 tide (solid line) are always larger than those of the M_2 tide (dashed line), which could explain why most of the deduced phase shifts of the O_1 tide are larger than the on-site phase shifts in Figure 5, below, whereas most of the deduced phase shifts of the M_2 tide are smaller than the on-site phase shifts in Figure 5, above for wells XY and BD.

5.1.2. Special Case of Well HZ for the Deduced Phase Shifts Induced by $K' = 0$

At small K' ($<10^{-7}$ m/s) in well HZ, the deduced/predicted phase shift becomes "flat" against K' and is thus no longer sensitive to model parameters (Y. Zhang et al., 2021). This may explain the significant uncertainties

Figure 10. Shale core from Jiao-Shi-Ba, Chongqing province (W. H. Zhang et al., 2016), with obvious layers.

in the inverted *T* (fig. 5 of Y. Zhang et al. (2021)) corresponding to the significant uncertainties in the on-site phase shifts in well HZ (Figure 4) with a nearly unchanged *K'* (none leakage, values of 10^{-10} (m/s) were assigned).

Meanwhile, for the same variation of the parameter *T* of well HZ, the variation in the phase shift for the O_1 tide (solid line in Figure 9) is significantly smaller than that for the M_2 tide (dashed line in Figure 9). In addition, even with 2 orders of magnitude of the variation of *K'*, the variation of phase shifts for the O_1 tide at well HZ is significantly smaller than that at the other wells (Figure 9). This could explain why the variation of the deduced phase shifts for the O_1 tide (Figure 5, below [red dots]) at well HZ are smaller, and the phase shifts are close to a straight line. This also may have induced the significant difference between the deduced phase shifts (red dots in Figure 5, below) and the on-site phase shifts (black dots in Figure 5, below) for the O_1 tide, which is attributed to the unconstrained analytical solution.

5.2. Influence of Aquifer Lithologies on the Phase Shifts

Sedimentary rocks are heterogeneous porous media containing complex distributions of heterogeneities (e.g., fluid patches and cracks) (Zhao et al., 2016, 2021). Due to the compact grain structure of shale, its permeability is low, which is approximately 10^{-4} to 10^{-3} mD (Chen et al., 2013; Li et al., 2013). Shale is characterized by low porosity/permeability, anisotropy (layered; Figure 10), and brittle (W. H. Zhang et al., 2016). For shale layers, horizontal permeability is significantly greater than vertical permeability (Du et al., 2019; S. Hu et al., 2020).

In the tidal response leaky model (two-layer model) (Wang et al., 2018), both the aquifer and aquitard are assumed to be isotropic and homogeneous, and the storage in the aquitard is neglected, implying a time constant for the aquitard to reach hydraulic equilibrium in a time shorter than the period of the tidal or barometric forcing. In addition, in the aquitard, all rocks are compressed tightly, without water, and with relatively low porosity/permeability. Thus, because the difference between the other rocks in the aquitard and shale (or mudstone also with low porosity/permeability) is small, the influence of shale or mudstone in the aquitard can be ignored. Therefore, shale or mudstone in the aquitard (Figure 3, GC well) does not cause obvious anisotropy or heterogeneity to the on-site aquitard lithology and has not caused obvious deviated phase shifts in well GC (Figure 5), indicating that the ideal leaky model could be perfectly matched in this well.

On the other hand, for the aquifer, because of the low permeability (porosity) of shale, water tends to go through other aquifer lithologies with relatively significant porosities or fractures rather than shale layers. Therefore, the shale content in the aquifer is regarded as the main effect causing anisotropy or heterogeneity.

Therefore, when the shale content in the aquifer is 0 or very small, for example, in well GC (aquifer shale content 0%), the influence of shale could be ignored and there is no anisotropic characteristic. Thus, the tidal response leaky model could be perfectly matched (Figure 5), and the original on-site phase shifts and the deduced phase shifts from the theoretical (analytical) model are mostly in accordance (Figure 5). However, when the shale content is very large, for example, in well XY (aquifer shale content 23.33%) and BD (aquifer shale content 40.09%), there is an obvious anisotropic characteristic, which is attributed to the anisotropic characteristic of shale or the improved layer structure (inhomogeneous) of the entire aquifer induced by the compact shale layers. Therefore, the tidal response leaky model could not be perfectly matched, and there are obvious deviations between the on-site phase shifts and deduced phase shifts from the theoretical (analytical) model (Figures 5 and 6). Meanwhile, according to the analytical solution, the phase shift of the O_1 wave should always be larger than that of the M2 wave (Q. Y. Yang et al., 2021), and most of the dots for well XY (aquifer shale content 23.33%) and BD (aquifer shale content 40.09%) deviate from this rule (Figure 4), because of the large amount of shale in the aquifer.

While, well HZ is an exception (aquifer shale content 6.98%) because of the extremely small value of K', leading to an unconstrained analytical solution.

5.3. Groundwater Exploitation

The water levels of the wells show a decreasing pattern from 2008 to 2011, probably induced by the groundwater exploitation on the North China Platform, which includes one shallow unconfined aquifer ((40–60 m) and three deep confined aquifers of different depths (120–170, 250–350, and 400–600 m) (Sakura et al., 2003), and the groundwater exploitation in North China is always above the depth of 400 m (H. F. Yang et al., 2021). However, groundwater exploitation is not the key point of this study, and we may discuss it in future studies.

6. Conclusion

Even a small amount of shale (~≥5%) in aquifer lithology might induce obvious anisotropy of the aquifer, and because of the low porosity/permeability of shale layers (anisotropy, extremely low porosity/permeability; approximately 10^{-4} to 10^{-3} mD), the entire aquifer may also be inhomogeneous, impacting the calculation results of isotropic and homogeneous models. This suggests that we should avoid setting observation aquifers onto shale lithology and that when the obtained results deviate from the ideal theoretical models with isotropic and homogeneous assumptions, there may be shale in the aquifer lithology. Furthermore, as found in this study, generally, the higher the shale content in aquifer lithology, the greater the phase shifts deviated for the tidal response leaky aquifer model.

Appendix A: Tidal Response Leaky Model

Assuming that the flow through the semi-confining aquitard is vertical and that the aquifer is laterally extensive, the tide-induced groundwater flow in the leaky aquifer may be evaluated by solving the following equation (Wang et al., 2018):

$$T\left[\frac{\partial^2 h}{\partial r^2}+\frac{1}{r}\frac{\partial h}{\partial r}\right]-\frac{K'}{b'}h=S\left(\frac{\partial h}{\partial t}-\frac{BK_{\mathrm{u}}}{\rho g}\frac{\partial \varepsilon_0}{\partial t}\right) \tag{A1}$$

The boundary conditions are

$$\begin{aligned} h(r,t)&=h_{\infty}(t)\ \text{at r}=\infty,\\ h(r,t)&=h_w(t)\ \text{at r}=r_{\mathrm{w}},\ \text{and}\\ 2\pi r_{\mathrm{w}}T(\partial h/\partial r)_{r=r_w}&=\pi {r_c}^2(\partial h_w/\partial t) \end{aligned} \tag{A2}$$

where h_w (m) $= h_{w,0}\, e^{i\omega t}$ denotes the periodic water level in the well, with complex amplitude $h_{w,0}$ (m); $\omega[\mathrm{s}^{-1}]$ denotes the angular frequency. ε_0 denotes the theoretical periodic solid-earth tidal strain, B denotes the Skempton

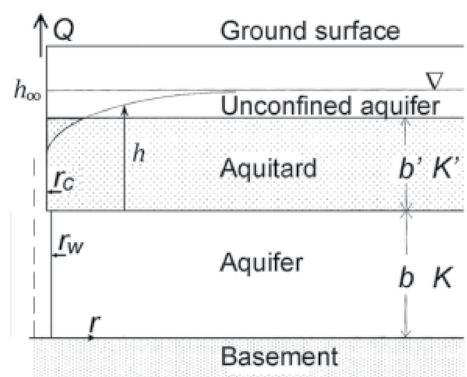

Figure A1. The leaky aquifer model by Wang et al. (2018). The vertical dashed line on the left indicates the position of the well axis located at $r = 0$. The thickness b and hydraulic conductivity K of the aquifer are related to aquifer transmissivity denoted by $T = bK$, the equivalent thickness and vertical hydraulic conductivity of the aquitard, denoted by b' and K', respectively (Wang et al., 2018).

coefficient, K_u denotes the bulk modulus, K' represents the vertical hydraulic conductivity of the aquitard, T represents the horizontal transmissivity of the aquifer, S represents the storage coefficient of the aquifer, b' represents the thickness of aquitard, r_c represents the case radius, and r_w represents the well radius.

After some assumptions and derivations, we have (Wang et al., 2018)

$$h_{w,0} = \frac{i\omega S}{((i\omega S + K'/b')\xi)}\left(\frac{BK_u\varepsilon_0}{\rho g}\right) \tag{A3}$$

The amplitude ratio and phase shift can be defined as

$$A = \mathrm{abs}\left(h_{w,0}/\frac{BK_u\varepsilon_0}{\rho g}\right) = \mathrm{abs}\left(\frac{i\omega S}{\left(i\omega S + \frac{K'}{b'}\right)\xi}\right) \tag{A4}$$

$$\eta = \arg\left(h_{w,0}/\frac{BK_u\varepsilon_0}{\rho g}\right) = \arg\left(\frac{i\omega S}{\left(i\omega S + \frac{K'}{b'}\right)\xi}\right) \tag{A5}$$

here

$$\xi = 1 + \left(\frac{r_c}{r_w}\right)^2 \frac{i\omega r_w}{2T\beta}\frac{K_0(\beta r_w)}{K_1(\beta r_w)} \tag{A6}$$

$$\beta = \left(\frac{K'}{Tb'} + \frac{i\omega S}{T}\right)^{\frac{1}{2}} \tag{A7}$$

where A represents the relative amplitude ratio of the water level to solid-earth tidal strain, η represents the phase shift, arg and abs represent the angle and magnitude of complex numbers, respectively, and K_n denotes the modified Bessel function of the second kind (Bessel function) with order n.

We can obtain the absolute amplitude ratio $A' = (h_{w,0}/\varepsilon_0)$ directly from the water level and solid-earth tides, so the equation set can be rewritten as

$$\begin{cases} A' = \mathrm{abs}\left(\dfrac{i\omega S}{\left(i\omega S + \dfrac{K'}{b'}\right)\xi}\right) * \dfrac{BK_u}{\rho g} \\ \eta = \arg\left(\dfrac{i\omega S}{\left(i\omega S + \dfrac{K'}{b'}\right)\xi}\right) \end{cases} \tag{A8}$$

where S, T, K', and BK_u are the unknown parameters. The original equation set contained four unknowns and two equations. We used both the M_2 and O_1 tidal responses (phase shifts and amplitude ratios) as the input to those equations; because the specific value of BK_u cannot be confirmed, we use the amplitude ratio of M_2 to divide that of O_1 to omit BK_u.

$$\begin{cases} A'_{M2}/A'_{O1} = \mathrm{abs}\left(\dfrac{i\omega_{M2}S}{\left(i\omega_{M2}S+\dfrac{K'}{b'}\right)\xi}\right)/\mathrm{abs}\left(\dfrac{i\omega_{O1}S}{\left(i\omega_{O1}S+\dfrac{K'}{b'}\right)\xi}\right) \\ \eta_{M2} = \arg\left(\dfrac{i\omega_{M2}S}{\left(i\omega_{M2}S+\dfrac{K'}{b'}\right)\xi}\right) \\ \eta_{O1} = \arg\left(\dfrac{i\omega_{O1}S}{\left(i\omega_{O1}S+\dfrac{K'}{b'}\right)\xi}\right) \end{cases} \tag{A9}$$

The phase (Figure A1) shifts of the M_2 and O_1 tidal responses of water level and the amplitude ratio of M_2 wave to O_1 wave were used as the three inputs, which were used to obtain those three parameters (S, T, and K'). Finally, the best solution for each well was obtained by least squares optimal fitting (Y. Zhang et al., 2021).

Conflict of Interest

The authors declare no conflicts of interest relevant to this study.

Data Availability Statement

Groundwater-level data used in this study were from the Groundwater Monitoring Network of the China Earthquake Networks Center (https://doi.org/10.12197/2022GA033).

Acknowledgments
The authors thank the China Earthquake Administration for providing the data used in this study. The authors are deeply grateful to Professor Chi-yuen Wang and Doctor Bo-ye Fu for the instructive suggestions and discussions and thank Qiu-ye Yang for the plotting of Figure 5. The research was supported by the National Natural Science Foundation of China (41874161 and 42141009) and the Youth Innovation Promotion Association Foundation of the Chinese Academy of Sciences (2019069).

References

Anyim, K., & Gan, Q. (2020). Fault zone exploitation in geothermal reservoirs: Production optimization, permeability evolution and induced seismicity. *Advances in Geo-Energy Research*, *4*(1), 1–12. https://doi.org/10.26804/ager.2020.01.01

Barbour, A. J., Xue, L., Roeloffs, E., & Rubinstein, J. L. (2019). Leakage and increasing fluid pressure detected in Oklahoma's wastewater disposal reservoir. *Journal of Geophysical Research: Solid Earth*, *124*(3), 2896–2919. https://doi.org/10.1029/2019JB017327

Beaumont, C., & Berger, J. (1975). An analysis of tidal strain observations from the United States of America: I. The laterally homogeneous tide. *Bulletin of the Seismological Society of America*, *65*(6), 1613–1629. https://doi.org/10.1785/bssa0650061613

Cai, J., Wei, W., Hu, X., Liu, R., & Wang, J. (2017). Fractal characterization of dynamic fracture network extension in porous media. *Fractals*, *25*(2), 1750023. https://doi.org/10.1142/s0218348x17500232

Chen, Q., Liu, H., Wang, S., Wang, L. S., Liu, J. Q., & Yang, B. (2013). Experimental study of the fundamental physical properties on shale in Longmaxi Formation of Lower Silurian, Chongqing. *Science Technology and Engineering*, *13*(15), 1671–1815.

Deng, Q. D., Zhang, P. Z., & Ran, Y. K. (2004). *Distribution of active faults in China (1:4000000)*. Science Press. (In Chinese).

Detournay, E., & Cheng, A. H. D. (1993). Chapter 5: Fundamentals of poroelasticity. In C. Fairhurst (Ed.), *Comprehensive rock engineering: Principles, practice and projects, Analysis and Design Method* (Vol. II, pp. 113–171). Pergamon Press.

Doan, M. L., Brodsky, E. E., Prioul, R., & Signer, C. (2006). *Tidal analysis of borehole pressure: A tutorial* (pp. 1–61). University of California.

Du, J., Hu, S., Pang, Z., Lin, S., Hou, L., & Zhu, R. (2019). The types, potentials and prospects of continental shale oil in China. *China Petroleum Exploration*, *24*(5), 560–568.

Hantush, M. S. (1960). Modification of the theory of leaky aquifers. *Journal of Geophysical Research*, *65*(11), 3713–3725. https://doi.org/10.1029/JZ065i011p03713

Hantush, M. S. (1967). Flow of groundwater in relatively thick leaky aquifers. *Water Resources Research*, 3(2), 583–590. https://doi.org/10.1029/wr003i002p00583

Hantush, M. S., & Jacob, C. E. (1955). Non-steady Green's functions for an infinite strip of leaky aquifers. *Transactions - American Geophysical Union*, *36*(1), 101. https://doi.org/10.1029/TR036i001p00101

Hsieh, P. A., Bredehoeft, J. D., & Farr, J. M. (1987). Determination of aquifer transmissivity from Earth tide analysis. *Water Resources Research*, *23*(10), 1824–1832. https://doi.org/10.1029/WR023i010p01824

Hu, C. L., Zhang, Y. F., Wang, Z. F., Li, J. J., & Zhang, H. B. (2014). Shale features and exploration prospect of shale gas in Longmaxi formation in northern Guizhou. *Special Oil and Gas Reservoirs*, *21*(4), 44–47.

Hu, S., Zhao, W., Hou, L., Zhi, Y., Rukai, Z., Songtao, W., et al. (2020). Development potential and technical strategy of continental shale oil in China. *Petroleum Exploration and Development*, *47*(4), 819–828.

Hussein, M. E. A., Odling, N. E., & Clark, R. A. (2013). Borehole water level response to barometric pressure as an indicator of aquifer vulnerability. *Water Resources Research*, *49*(10), 7102–7119. https://doi.org/10.1002/2013WR014134

Li, Y. J., Liu, H., Zhang, L. H., Lu, Z. G., Li, Q. R., & Huang, Y. B. (2013). Lower limits of evaluation parameters for the lower Paleozoic Longmaxi shale gas in southern Sichuan Province. *Science China Earth Sciences*, *56*(5), 710–717. https://doi.org/10.1007/s11430-013-4579-4

Lu, Y. Z., Li, S. L., Deng, Z. H., Pan, H. W., Che, S., & Li, Y. L. (2002). *Seismology analysis and prediction system based on GIS (Mapseis Software)* (pp. 1–124). Chengdu Map Press. (in Chinese).

Rojstaczer, S. (1988). Determination of fluid flow properties from the response of water levels in wells to atmospheric loading. *Water Resources Research*, *24*(11), 1927–1938. https://doi.org/10.1029/WR024i011p01927

Sakura, Y., Tang, C., Yoshioka, R., & Ishibashi, H. (2003). Intensive use of groundwater in some areas of China and Japan. In M. R. Llamas & E. Custodio (Eds.), *Intensive use of groundwater: Challenges and opportunities*. Balkma.

Seismic Monitoring Records of China. (2002). *Seismic monitoring records of China*. Seismological Press. (in Chinese).

Wang, C. Y., Doan, M. L., Xue, L., & Barbour, A. J. (2018). Tidal response of groundwater in a leaky aquifer—Application to Oklahoma. *Water Resource Research*, *54*(10), 8019–8033. https://doi.org/10.1029/2018WR022793

Wang, C. Y., & Manga, M. (2021). *Water and earthquake*s. Springer-Nature.

Wang, H. F. (2000). *Theory of linear poroelasticity* (p. 62). Princeton University Press.

Yang, H. F., Cao, W. G., Zhi, C. S., Li, Z. Y., Bao, X. L., Ren, Y., et al. (2021). Evolution of groundwater level in the North China Plain in the past 40 years and suggestions on its overexploitation treatment. *Geology in China*, *48*(4), 1142–1155. (in Chinese with English abstract).

Yang, Q. Y., Zhang, Y., Fu, L. Y., Ma, Y. C., & Hu, J. H. (2021). Vertical leakage occurred after an earthquake: Suggestions for utilizing the mixed flow model. *Lithosphere*, *2021*(Special 3), 8281428.

Zhang, H., Shi, Z., Wang, G., Sun, X., Yan, R., & Liu, C. (2019). Large earthquake reshapes the groundwater flow system: Insight from the water-level response to earth tides and atmospheric pressure in a deep well. *Water Resource Research*, *55*(5), 4207–4219. https://doi.org/10.1029/2018WR024608

Zhang, W. H., Fu, L. Y., Zhang, Y., & Jin, W. J. (2016). Computation of elastic properties of 3D digital cores from the Longmaxi shale. *Applied Geophysics*, *13*(2), 364–374. https://doi.org/10.1007/s11770-016-0542-4

Zhang, Y., Sun, X. L., Huang, T. M., Qi, S. W., Fu, L. Y., Yang, Q. Y., et al. (2022). Possible continuous vertical water leakage of deep aquifer: Records from a deep well in Tianjin province, North China. *Geofluids*, *2022*, 4419310.

Zhang, Y., Wang, C. Y., Fu, L. Y., & Yang, Q. Y. (2021). Are deep aquifers really confined? Insights from deep groundwater tidal responses in the North China Platform. *Water Resources Research*, *57*(11), e2021WR030195. https://doi.org/10.1029/2021WR030195

Zhang, Y., Wang, C. Y., Fu, L. Y., Zhao, B., & Ma, Y. C. (2019). Unexpected far-field hydrological response to a great earthquake. *Earth and Planetary Science Letters*, *519*, 202–212. https://doi.org/10.1016/j.epsl.2019.05.007

Zhao, L. X., Qin, X., Zhang, J. Q., Liu, X. W., Han, D. H., Geng, J., & Xiong, Y. (2018). An effective reservoir parameter for seismic characterization of organic shale reservoir. *Surveys in Geophysics*, *39*(3), 509–541. https://doi.org/10.1007/s10712-017-9456-9

Zhao, L. X., Wang, Y., Yao, Q., Geng, J., Li, H., Yuan, H., & Han, D. (2021). Extended Gassmann equation with dynamic volumetric strain: Modeling wave dispersion and attenuation of heterogenous porous rocks. *Geophysics*, *86*(3), MR149–MR164. https://doi.org/10.1190/geo2020-0395.1

Zhao, L. X., Yao, Q., Han, D., Yan, F., & Nasser, M. (2016). Characterizing the effect of elastic interactions on the effective elastic properties of porous, cracked rocks. *Geophysical Prospecting*, *64*(1), 157–169. https://doi.org/10.1111/1365-2478.12243

Zhu, A. Y., & Wang, C. Y. (2020). Response of leaky aquifers to Earth tides—Interpreted with numerical simulation. *Journal of Hydrology*, *581*, 124458. https://doi.org/10.1016/j.jhydrol.2019.124458